Journal of Zhejiang University-SCIENCE A (Applied Physics & Engineering) 2025 26(3):177-193
www.jzus.zju.edu.cn; www.springer.com/journal/11582
E-mail: jzus_a@zju.edu.cn

Research Article

https://doi.org/10.1631/jzus.A2400216

Hydraulic conductivity of sand influenced by temperature and porosity in centrifugal tests

Jianjian HE, Xihao JIANG, Yubing WANG✉

Center for Hypergravity Experiment and Interdisciplinary Research, College of Civil Engineering and Architecture, Zhejiang University, Hangzhou 310058, China

Abstract: This study focused on the hydraulic conductivity of sand in centrifuge modeling. A self-designed temperature-controlled falling-head permeameter apparatus was used, and a series of falling-head seepage tests were performed on sand samples with various porosities at different temperatures and centrifugal accelerations. The objectives were to qualitatively and quantitatively investigate the effects of temperature, porosity, and centrifugal acceleration on the hydraulic conductivity of sand and to study the applicability of the Kozeny-Carman equation for the centrifugal environment. Test results showed that in a similar temperature range and under the same porosity, the hydraulic conductivity of the sand is linearly correlated with centrifugal acceleration. When subjected to the same centrifugal acceleration and in a similar temperature range, the hydraulic conductivity of the sand exhibits an almost linear increase in relation to its porosity function ($s^3/(1-s)^2$); the functional relationships between the hydraulic conductivity of the sand and temperature, centrifugal acceleration level, and porosity were established using two pathways. When the centrifugal acceleration is less than 50*g*, the Kozeny-Carman equation is effectively accurate in predicting the hydraulic conductivity of sand; however, when the centrifugal acceleration exceeds 50*g*, it is important to consider a significant error.

Key words: Hydraulic conductivity of sand; Temperature; Porosity; Centrifugal acceleration; Kozeny-Carman equation

1 Introduction

The physical model test is a fundamental research approach in geotechnical engineering, and centrifuge modeling is a significant experimental technique within the physical model test. Due to its capacity to accurately replicate the stress state of a prototype, ensuring consistency in the deformation and failure mechanisms between the model and the prototype (Chen et al., 2011), centrifuge modeling is commonly favored as an experimental technique (Ng, 2014). Many centrifuge model tests are related to seepage, such as those of rainfall-induced landslides (Ling and Ling, 2012; Chen YL et al., 2019), dam breaches (Mei et al., 2022; Zhang et al., 2023), seepage behavior of dams (Wang et al., 2013; Ye et al., 2021), and contaminant migration (Zeng et al., 2022; Zheng et al., 2022). Therefore, in-depth research on the seepage characteristics of soils in a centrifugal environment is of great significance for solving various seepage-related geotechnical engineering problems.

Permeability is a crucial engineering property of soil (Joshaghani and Ghasemi-Fare, 2021). The hydraulic conductivity is a specific characterization of the permeability of soil, and is an essential parameter for studying the seepage field and assessing the deformation and stability of geotechnical structures when subjected to water-related factors like rainfall and changes in water level (Su et al., 2014). Therefore, many researchers have conducted in-depth studies on the hydraulic conductivity of soil in a 1*g* (*g* is the acceleration of gravity) environment (Cho et al., 1999; Wang et al., 2010; Ye et al., 2013; Ng and Coo, 2015). There are many factors that influence the hydraulic conductivity of soil, such as the porosity (Su et al., 2014; Li et al., 2024), particle shape (Wang et al., 2017; Li et al., 2024), particle size distribution (Su et al., 2014; Wang et al., 2017), temperature (Ye et al., 2013; Joshaghani and Ghasemi-Fare, 2021), and impact load (Li et al.,

✉ Yubing WANG, wangyubing@zju.edu.cn
Jianjian HE, https://orcid.org/0000-0002-8583-1641
Yubing WANG, https://orcid.org/0000-0002-2398-6007

Received Apr. 24, 2024; Revision accepted June 14, 2024; Crosschecked Feb. 24, 2025

2024). While there has been little research on the factors that affect the hydraulic conductivity of soil in centrifuge modeling, a significant amount of research has been dedicated to validating the scaling law of hydraulic conductivity in theory (Schofield, 1980; Tan and Scott, 1985, 1987; Butterfield, 2000; Thusyanthan and Madabhushi, 2003). Some scholars have used experimental methods to verify the scaling law of hydraulic conductivity (Singh and Gupta, 2000; Wang et al., 2011; van Tonder and Jacobsz, 2017). That is, by testing the hydraulic conductivity of soil in a centrifugal environment (k_{cen}) and comparing it with the hydraulic conductivity of a 1*g* scale (k_p), the scaling ratio of hydraulic conductivity (k_{cen}/k_p) can be obtained. However, these researchers have found that the k_{cen}/k_p obtained from experiments is not equal to the theoretical scaling law. The reasons for this phenomenon may involve the insufficient length of the centrifuge arm, non-uniformity of the centrifugal acceleration field, soil consolidation, and other factors (Sharma and Samarasekera, 2007; Wang et al., 2011). However, we believe that another possible reason for this phenomenon is the lack of temperature control on the model during the experimental process, as the hydraulic conductivity is significantly influenced by temperature. In the above studies, the measurement of the hydraulic conductivity of soil was not rigorous enough and so the influence of temperature on hydraulic conductivity was neglected. Therefore, studies of the effect of temperature on hydraulic conductivity in centrifuge modeling are needed and are of great significance for improving the fundamental theory of centrifuge modeling.

In addition, the coupled temperature-hydraulic-mechanical (THM) behavior of soil has become one of the main focuses and challenges in geotechnical engineering in recent years, and is relevant for applications such as underground energy engineering (Sailer et al., 2021), natural gas hydrate exploitation (Ye et al., 2022), and nuclear waste disposal (Zhao et al., 2016). Centrifuge modeling has also been extensively used to investigate these challenges (Ng et al., 2021; Wang et al., 2022). The hydraulic conductivity of soil is one of the crucial parameters for accurately describing the coupled THM behavior of soil. For example, Xiong (2018) used COMSOL software to analyze the thermo-hydro coupling in saturated sand, building upon prior centrifuge test results, and found that in a centrifugal environment, hydraulic conductivity has a substantial influence on the thermo-hydro coupling effect in saturated soil. Nevertheless, researchers have not adequately addressed the influence of temperature on hydraulic conductivity in a centrifugal environment. This deficiency may have had a negative impact on the precise replication of soil THM coupling behavior by centrifuge modeling. Therefore, accurately revealing and characterizing the influence of temperature on the hydraulic conductivity of soil in a centrifugal environment is crucial for using centrifuge modeling to accurately depict the coupled THM behavior of soil and is also of significant importance for addressing multifield coupling problems in geotechnical engineering.

The experimental measurement of soil hydraulic conductivity exhibits remarkable accuracy and extensive practicality. Nevertheless, the process of experimentally determining soil hydraulic conductivity can be laborious and time-consuming. Consequently, numerous scholars have proposed theoretical prediction equations for soil hydraulic conductivity based on the soil's inherent properties and a large amount of experimental data (Aubertin et al., 1996; Chapuis, 2004; Li et al., 2023; Zhong et al., 2023; Fan and Rowe, 2024). The Kozeny-Carman hydraulic conductivity prediction equation (hereinafter referred to as the Kozeny-Carman equation) (Carman, 1939; Nomura et al., 2018) is widely used. The applicability of the hydraulic conductivity prediction equations mentioned above has been extensively confirmed in a 1*g* environment. Nevertheless, few studies have considered the suitability of these hydraulic conductivity prediction equations in a centrifugal environment. Also, no equation for predicting soil hydraulic conductivity has been proposed that is acceptable for a centrifugal environment.

Sand is a common material found in many geotechnical structures, including dams (Wen et al., 2015; Eisma and Merwade, 2020; Li et al., 2021), embankments (Zhao et al., 2021; Ikbarieh et al., 2023; Qin et al., 2024), tunnel strata (Yang et al., 2021; Cheng et al., 2023; Khalajzadeh et al., 2023), and foundation pits (Li et al., 2018; Sun et al., 2019; Gao et al., 2023). Therefore, it is meaningful for the safety of geotechnical structures to investigate the centrifugal hydraulic conductivity of sand, considering the effects of various influencing factors. However, previous studies (Singh and Gupta, 2000; Wang et al., 2011; van Tonder and Jacobsz, 2017) focused mainly on clay, with little research on sand. Thus, in this study, we used a self-designed

apparatus to conduct centrifuge modeling, and a series of falling-head seepage tests were performed on sand samples with various porosities at different temperatures and centrifugal accelerations. The main aims of this study were: (1) to investigate the effects of temperature, porosity, and centrifugal acceleration on the hydraulic conductivity of sand; (2) to establish quantitative relationships between hydraulic conductivity, temperature, porosity, and centrifugal acceleration; (3) to verify the applicability of the Kozeny-Carman equation for a centrifugal environment.

2 Experimental setup

2.1 Test setup

To conduct seepage tests at different temperatures in a centrifugal environment, a self-designed temperature-controlled falling-head permeameter apparatus was used. A schematic view of the apparatus is shown in Fig. 1. This paper simply provides a brief introduction to the apparatus. The temperature-controlled falling-head permeameter is the core component of the apparatus. It is used to regulate the temperature of soil samples and fluids and conduct falling-head tests. The rest of the apparatus is linked to the temperature-controlled falling-head permeameter as follows:

(1) The pore water pressure transducer module consists of several pore water pressure transducers that are linked to pore water pressure monitoring channels (not marked in Fig. 1) located on the base pedestal of the temperature-controlled falling-head permeameter. The soil column cylinder has several pore water pressure monitoring holes, which are numbered as Hole 1, Hole 2, Hole 3, and Hole 4 (Fig. 1). The soil column cylinder is separated into two sections: the 160-mm-tall soil sample area is located below, and the 145-mm-tall fluid area is located above. The center of Hole 4 is positioned 30 mm above the bottom of the soil sample; the distance between the centers of Hole 3 and Hole 4, as well as that between the centers of Hole 3 and Hole 2, is 50 mm; the distance between the centers of Hole 1 and Hole 2 is 35 mm. A total of five pore water pressure transducers were used in this study. To accurately measure the water level in the fluid area, two pore water pressure transducers, labeled $P_{1\text{-}1}$ and $P_{1\text{-}2}$ respectively, were placed in Hole 1. One pore water pressure transducer was installed at each of Hole 2, Hole 3, and Hole 4, labeled P_2, P_3, and P_4, respectively. The accuracy of all the pore water pressure transducers was 0.2%.

(2) The temperature transducer module has several temperature transducers positioned on the top cap of the permeameter. Three temperature transducers

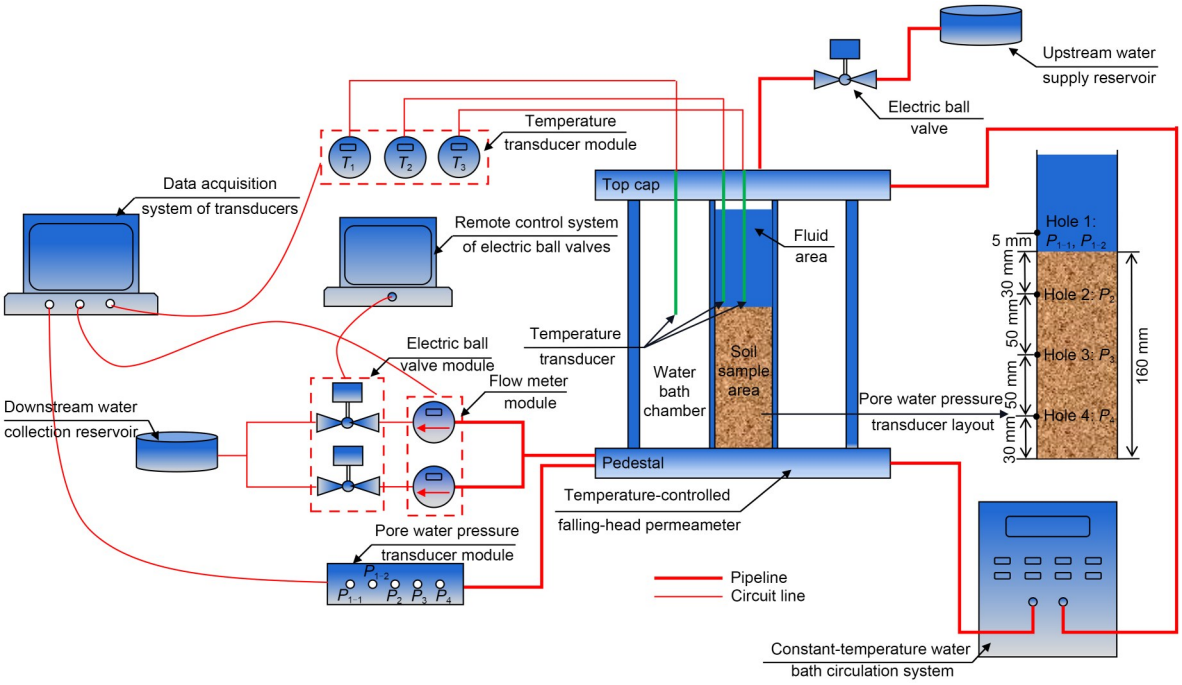

Fig. 1 Schematic view of the temperature-controlled falling-head permeameter apparatus

were used in this study, labeled T_1, T_2, and T_3, respectively. T_1 was positioned at the center of the water bath chamber to monitor the temperature of the water bath chamber. T_2 was located at the edge of the fluid area, near the wall of the soil column cylinder, to monitor the temperature of the fluid at the edge of the fluid area. T_3 was positioned in the middle of the fluid area to monitor the temperature of the center of the fluid area. The measurement range for T_1, T_2, and T_3 was from −50 to 50 °C.

(3) On the base pedestal of the permeameter, there is a flow monitoring channel (not marked in Fig. 1), which is linked to several flow meters in the flow meter module.

(4) The electric ball valve module consists of multiple electric ball valves, with some being connected in series with flow meters so that tests can be started and stopped remotely. These electric ball valves are also connected to a downstream water collection reservoir, which is used to collect seepage fluid. In addition, an electric ball valve is connected in series with the upstream water supply reservoir, which provides seepage fluid to the fluid area.

(5) To regulate the temperature of soil samples and fluids, the temperature-controlled falling-head permeameter's top cap and base pedestal are equipped with water bath channels (not marked in Fig. 1) that are connected to the constant-temperature water bath circulation system.

(6) The centrifuge's transducer data acquisition system measures and gathers information from the transducers. Moreover, a computer can be used to remotely operate the electric ball valves.

2.2 Test materials and test plan

Fig. 2 shows the particle size distribution of the test soil. The test soil, with particle sizes ranging from 0.075 to 0.25 mm, was separated from China ISO standard sand. Its specific gravity was 2.631, with a maximum void ratio of 0.956 and a minimum void ratio of 0.589. Deaired water was used as the seepage fluid.

A total of 36 groups of tests were carried out in a centrifugal environment (Table 1). Table 1 shows the temperatures for the tests. The test temperatures represent the actual test temperatures for the soil samples, while the set temperatures indicate the desired set temperatures for the constant-temperature water bath circulation system (Fig. 1) to achieve the corresponding test temperatures of the soil samples.

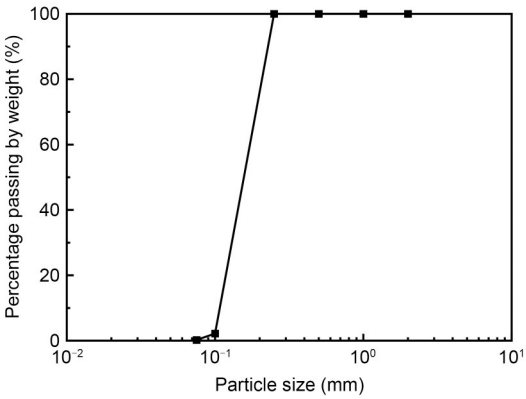

Fig. 2 Particle size distribution curve of test soil

Table 1 Temperatures for the tests

Centrifugal acceleration	Temperature (°C)					
	s=0.381		*s*=0.420		*s*=0.458	
	Test	Set	Test	Set	Test	Set
15*g*	13.2	10.5	12.7	9.0	13.0	10.0
	23.2	22.5	21.6	19.0	22.5	20.0
	32.7	33.5	32.2	31.0	32.4	31.0
	42.2	45.0	42.2	42.0	43.5	42.5
30*g*	16.0	10.5	12.7	9.0	13.6	10.0
	26.4	26.0	21.3	19.0	22.2	20.0
	36.4	37.5	31.8	31.0	32.2	31.0
	45.3	48.5	41.2	42.0	42.4	42.5
50*g*	18.9	10.5	12.8	9.0	13.8	10.0
	29.2	29.0	21.5	19.0	22.3	20.0
	39.0	40.5	32.0	31.0	32.2	31.0
	49.2	53.0	41.2	42.0	42.5	42.5

s represents the porosity

Table 1 shows that, for the soil sample with a porosity of 0.381, the temperature settings for the constant-temperature water bath circulation system differed significantly from the temperature settings for the soil samples with the other two porosities. The reason for this discrepancy is that we conducted that test in the summer (early July), while we conducted the other two tests in the spring (early April). In summer, the temperature control efficiency of the constant-temperature water bath circulation system is lower than that in spring, especially for low-temperature control. For instance, if we set the constant-temperature water bath circulation system to 10.5 °C for the soil sample with a porosity of 0.381, we could control the soil sample test temperatures to 13.2, 16.0, and 18.9 °C at 15*g*, 30*g*, and 50*g*, respectively. This was mainly because in summer, the greater the centrifugal acceleration, the

higher the rotational speed of the centrifuge, resulting in increased heat generation. Consequently, the low-temperature control effectiveness of the water bath circulation system diminished. Therefore, although the constant-temperature water bath circulation system was set to 10.5 ℃, it could maintain the soil sample test temperatures at only 13.2, 16.0, and 18.9 ℃ at 15*g*, 30*g*, and 50*g*, respectively. The soil samples with porosities of 0.420 and 0.458 did not exhibit this phenomenon.

Table 1 also shows that, during high-temperature control, although the greater centrifugal acceleration results in increased heat generation due to the higher rotational speed of the centrifuge, it also enhances the convection, which ensures that the temperature regulated at higher centrifugal acceleration remains relatively close to that at lower centrifugal acceleration, as well as to the target set temperature. Thus, compared to lower centrifugal acceleration, higher centrifugal acceleration leads to higher temperature control efficiency of the constant-temperature water bath circulation system. For example, if we set the constant-temperature water bath circulation system to 42.0 ℃ for the soil sample with a porosity of 0.420, we could adjust the soil sample test temperatures to 42.2, 41.2, and 41.2 ℃ for 15*g*, 30*g*, and 50*g*, respectively. We observed the same phenomenon in the soil sample with a porosity of 0.458. The relative density of the sand used in the experiment was 0.93, 0.63, and 0.30, respectively, corresponding to void ratios of 0.615, 0.725, and 0.846 and corresponding porosities of 0.381, 0.420, and 0.458, respectively.

2.3 Test preparation in a 1*g* environment

Several test preparations were completed in a 1*g* environment, including the following steps:

(1) Preparation of a soil sample. The sand was oven-dried and subsequently used to make the samples using the dry tamping method (Zhu et al., 2021). Each soil sample had a diameter of 60 mm and a height of 160 mm. It was compacted into eight layers, each 20 mm thick.

(2) Saturation of the soil sample. Each soil sample was saturated in two stages: first with carbon dioxide for 3 h and then with airless water for 12 h.

(3) Installation of the model. After saturation, the temperature-controlled falling-head permeameter and other equipment were placed in the model box. Then, the model box was installed in the centrifuge (Fig. 3).

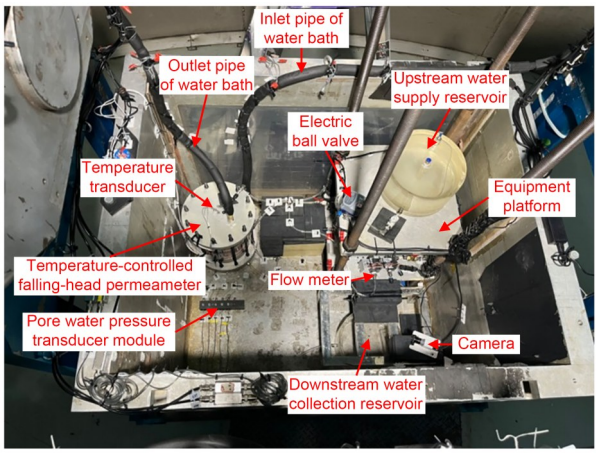

Fig. 3 Apparatus after installation in the ZJU400 centrifuge

(4) Regulation of soil sample temperature. Following the installation of the model, the water bath circulation system was turned on to regulate the fluid and soil sample temperatures at the desired levels.

2.4 Test procedure in a centrifugal environment

Experiments were carried out using the ZJU400 centrifuge at Zhejiang University, China, which has a spinning radius of 4.5 m, a maximum centrifugal acceleration of 150*g*, a maximum capacity of 400 *g*·t, and a basket volume of 1.5 m×1.2 m×1.5 m. Once the temperature control procedure in a 1*g* environment was completed, the centrifuge was started. The test procedure for a single test was as follows:

(1) Step I: Fill the fluid area. The current test is marked as Test *N*. After Test *N* is completed, the downstream electric ball valve is shut, while the electric ball valve upstream of the upstream water supply reservoir is opened. Then, fluid is injected into the fluid area, and once full, the electric ball valve of the upstream water supply reservoir is closed.

(2) Step II: Adjust the temperature. After completing Step I, the water bath temperature is adjusted to the predetermined temperature for the subsequent test, which is labeled as Test *N*+1.

(3) Step III: Adjust the centrifuge acceleration. After completing Step II, adjust the centrifuge acceleration to the target value of Test *N*+1.

(4) Step IV: Test the apparatus's sealing. After completing Step III, monitor the values of all pore water pressure transducers. If the values remain stable, it indicates good sealing of the apparatus. Conversely, if the values change, it suggests water leakage in the

apparatus. In this study, based on the pore water pressure transducers' values, we inferred that the apparatus maintained good sealing under all experimental conditions.

(5) Step V: Conduct the test. After completing Step IV, carefully observe the readings of the three temperature transducers, and after reaching the target temperature for Test N+1, choose the suitable flow meter, activate the relevant electric ball valve to conduct the test, and then shut the ball valve after the test is finished.

Note that in this study, after a single test was completed, the soil sample was not refilled. This is because using a single sample can reduce the differences in soil properties caused by refilling, making the test results more comparable. The properties of soil samples are significantly influenced by the preparation process. In our tests, the soil samples needed to undergo four temperature ranges (around 13, 23, 33, and 43 ℃). We would have needed four samples if we were to perform refills after each temperature range. Ensuring that these four samples had very similar soil properties would have been a substantial challenge. From this perspective, using the same sample throughout the entire testing process offered greater control over the soil properties compared to refilling. This significantly enhanced the comparability of the test results obtained.

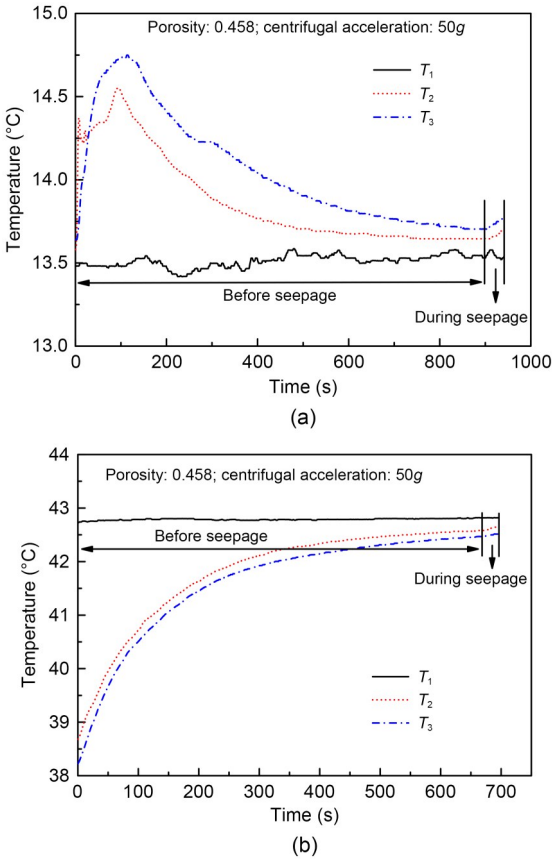

Fig. 4 Variation of water bath temperature (T_1) and fluid temperatures (T_2 and T_3) with time: (a) the experimental temperature was 13.8 ℃; (b) the experimental temperature was 42.5 ℃

3 Results and discussion

3.1 Temperature regulation

Fig. 4 shows the changes in water bath temperature (T_1) and fluid temperatures (T_2 and T_3) over time before and during seepage for a sand sample with a porosity of 0.458 in a 50g environment when the experimental temperatures were 13.8 and 42.5 ℃, which correspond to low- and high-temperature test conditions, respectively. Fig. 4 shows that, before seepage, the water bath circulation system consistently adjusted the fluid temperature and maintained it constant after reaching the desired temperature. Fig. 4 also indicates that although the fluid's temperature progressively rose during the seepage process, it did not exceed a 0.5 ℃ change during the entire seepage test, thereby meeting the test requirement that the apparatus can precisely control the temperatures of sand samples and fluids. The other tests gave the same results and so are not shown in this paper.

3.2 Seepage water head process line

When a falling-head seepage test is carried out, the seepage stability of the soil sample is directly reflected by the change in the seepage water head over time, which is called the seepage water head process line. Fig. 5 illustrates the variations in the seepage water head (h_1) over time of sand with various porosities under different temperatures and centrifugal accelerations. The values of seepage water head were calculated from the pore water pressure P_{1-1} or P_{1-2} (for calculation details, see Section 3.3.1). Fig. 5 shows that the seepage water heads of the three sand samples gradually decreased with time, and the rate of decline of each seepage water head process line was stable, indicating that the seepage of the samples under each test condition was stable and the results of each test were reliable. With the same porosity, the rate of decline of the seepage water head is related to factors such as centrifugal acceleration and temperature: the greater the

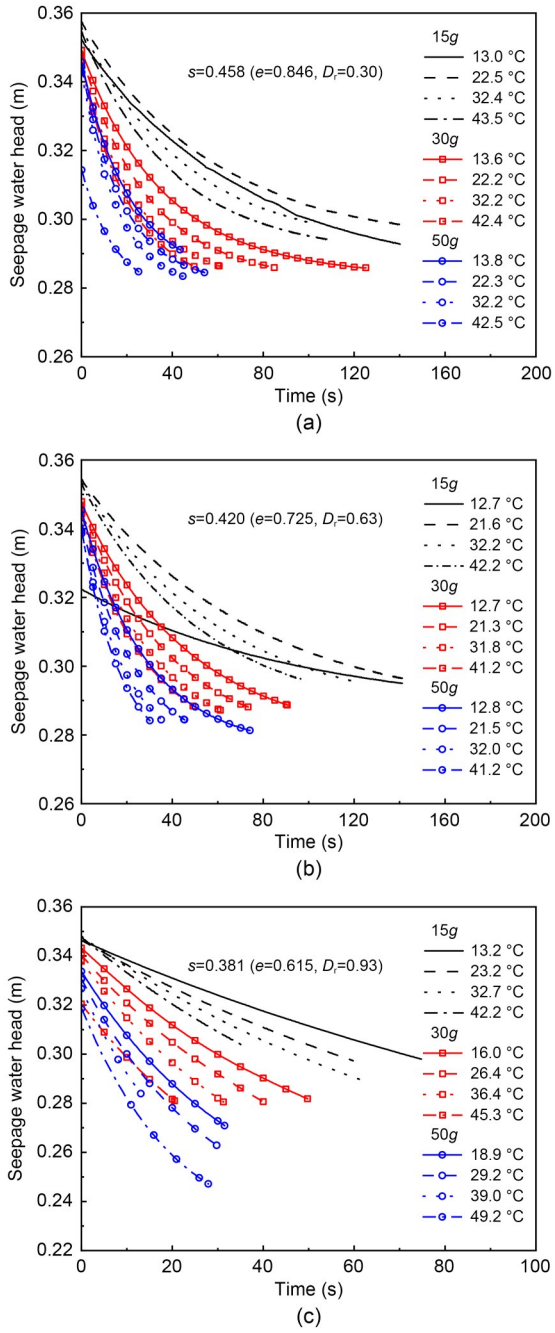

Fig. 5 Change in seepage water head of sand samples with time: (a) s=0.458; (b) s=0.420; (c) s=0.381. e is the void ratio of sand; D_r is the relative density of sand

centrifugal acceleration, the higher the temperature, and the higher the rate of decline. Although the seepage water head process lines of "15g, 13 °C" and "15g, 12.7 °C" in Figs. 5a and 5b differed somewhat from the others, this was due to the initial water head difference in these two tests being relatively low. This initial condition caused the rate of decrease in water head at the beginning of the test to be lower than those in the other tests.

3.3 Hydraulic conductivity

3.3.1 Calculation of hydraulic conductivity

The main focus of this study was on the hydraulic conductivity of the whole sand sample; we did not look into the layered hydraulic conductivity. Thus, the calculation of hydraulic conductivity was limited to the sand sample located between Hole 2 and Hole 4. The following equation was used to calculate each sand sample's hydraulic conductivity:

$$k_T=\frac{QL_0}{AHt}, \tag{1}$$

where k_T is the hydraulic conductivity at temperature T, cm/s; Q is the flow rate in t, cm^3; L_0 is the distance between the centers of two pore water pressure monitoring holes, cm; A is the cross-sectional area of the soil sample, cm^2; H is the total head difference between the centers of two pore water pressure monitoring holes, obtained by the relationship between the water head and the pore water pressure, cm; t is the test duration, s. When using Eq. (1), the seepage should satisfy Darcy's law. To check the validity of Darcy's law, we used the Reynolds number (Re): $Re=\rho vd/\mu$, where ρ is the fluid density, v is the seepage velocity, d is the soil characteristic microscopic length (such as the effective particle size d_{10}), and μ is the fluid dynamic viscosity coefficient (Singh and Gupta, 2000). Darcy's law is applicable to seepage through soils provided that the Re remains below 1. In the present study, the Re was calculated on the basis of d_{10} (which was 0.108 mm). The maximum value of Re of all tests was 0.90 (i.e., Re<1), which indicates the validity of Darcy's law in this study.

To calculate the total head difference H, it is necessary to convert the pore water pressure into the water head. The specific conversion process is as follows: When the soil column is positioned eccentrically, the calculation diagram of the total head at any point in the soil sample is as shown in Fig. 6. Given the non-uniformity of the centrifugal field and the eccentric positioning of the soil column, the centrifugal acceleration value N' at any given height of h_0 from plane E (which serves as the datum plane) in the soil sample is

$$N'=\frac{ng}{R}\sqrt{L^2+(R_0-h_0)^2}, \tag{2}$$

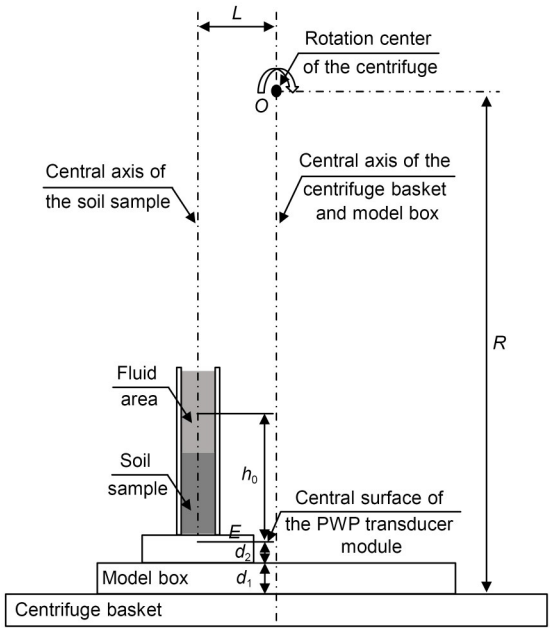

Fig. 6 Calculation diagram of the total head at any point in the sand sample. PWP: pore water pressure

where n is the centrifugal acceleration level; R is the maximum effective rotation radius of the centrifuge; L is the eccentricity distance; $R_0=R-d_1-d_2$; d_1 is the model box base thickness; d_2 is the distance between plane E and the top surface of the model box base. From Eq. (2), we can obtain the total head height of h_0 when the total pore water pressure is

$$P=\int_0^{h_0}\rho\frac{ng}{R}\sqrt{L^2+(R_0-h)^2}\,\mathrm{d}h. \tag{3}$$

Using Eq. (3), we used Matlab to solve the value of the total head corresponding to pore water pressure.

3.3.2 Changes in hydraulic conductivity with centrifugal acceleration under the same porosity

In this study, we adopted the viewpoint that the hydraulic conductivity of soil changes with centrifugal acceleration in centrifuge modeling (Singh and Gupta, 2000; Garnier et al., 2007; Wang et al., 2011). Fig. 7 illustrates how the hydraulic conductivity of sand with different porosities changed with centrifugal acceleration in a similar temperature range. The

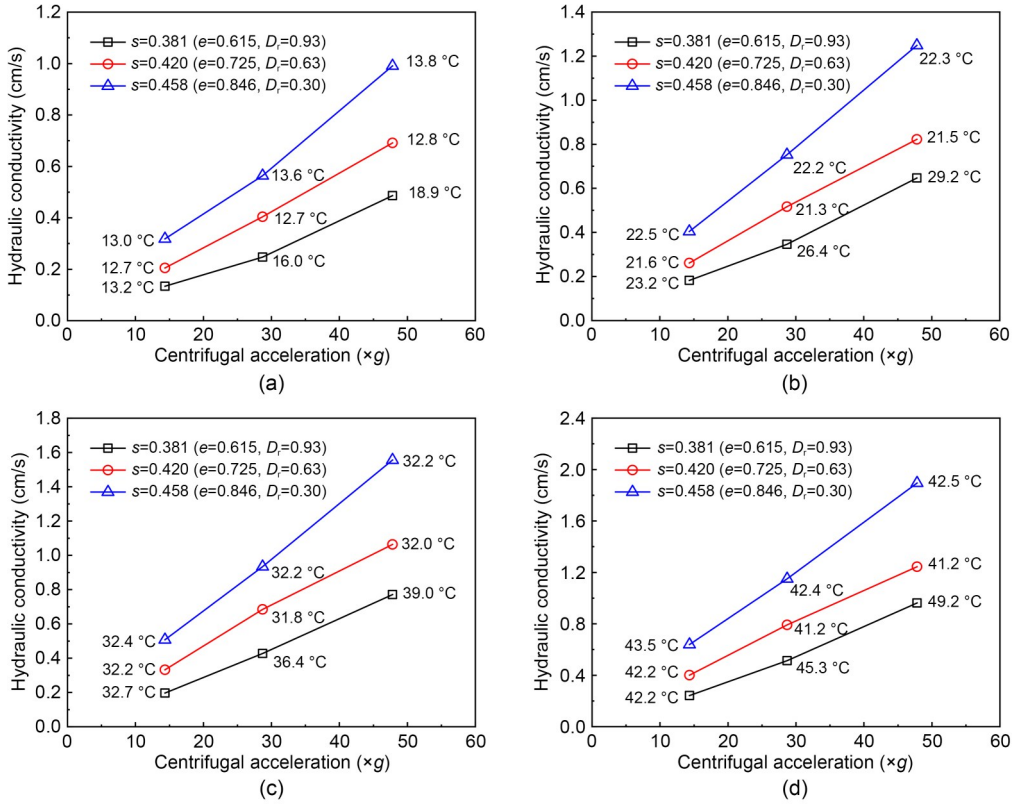

Fig. 7 Hydraulic conductivities of sand samples with different porosities varying with centrifugal acceleration in a similar temperature range: (a) around 13 ℃; (b) around 23 ℃; (c) around 33 ℃; (d) around 43 ℃

above-mentioned hydraulic conductivity is the hydraulic conductivity at real temperature, not at 20 ℃, and the temperature-controlled falling-head tests were conducted at about 13, 23, 33, and 43 ℃. The real temperature is the average temperature of the entire seepage process. Fig. 7 shows that in a similar seepage temperature range, no matter how dense the sand (the porosities of 0.381, 0.420, and 0.458 correspond to loose sand, medium dense sand, and dense sand, respectively, in this study), the hydraulic conductivity of the sand was linearly correlated with the centrifugal acceleration. In other words, the higher the centrifugal acceleration, the greater the hydraulic conductivity of sand, which is similar to the phenomenon that clay's hydraulic conductivity increases with increasing centrifugal acceleration (Wang et al., 2011).

3.3.3 Changes in hydraulic conductivity with porosity under the same centrifugal acceleration

The Kozeny-Carman equation can effectively predict the hydraulic conductivity of soil in a 1*g* environment, and one of its forms is as follows (Flint and Selker, 2003; Wang et al., 2011):

$$k=\frac{d_{\mathrm{m}}^2}{180}\frac{s^3}{(1-s)^2}\frac{\rho g}{\mu}, \tag{4}$$

where d_{m} is the characteristic particle size of the soil. Therefore, to establish the relationship between the hydraulic conductivity of sand and its porosity in a centrifugal environment, we introduce a porosity function based on the Kozeny-Carman equation. Specifically, we refer to $s^3/(1-s)^2$ in Eq. (4) as the porosity function.

We plotted the relationship between hydraulic conductivity and the porosity function ($s^3/(1-s)^2$) of sand in similar temperature ranges (around 13, 23, 33, and 43 ℃) under three centrifugal accelerations (15*g*, 30*g*, and 50*g*), as shown in Fig. 8. From Fig. 8, it can be observed that: (1) Under the same centrifugal acceleration and in a similar temperature range, the porosity of sand increased, and its hydraulic conductivity also increased, consistent with results from experiments conducted in a 1*g* environment (Su et al., 2014). This is because as porosity increases, the volume of pores within a unit volume of soil also increases. This leads to a larger cross-sectional area for fluid flow through the soil under the same hydraulic head pressure, resulting in an increase in hydraulic conductivity (Su et al., 2014). (2) Under the same centrifugal acceleration and in a similar temperature range, the hydraulic conductivity of sand showed a nearly linear growth in relation to its porosity function ($s^3/(1-s)^2$). This trend aligns with the findings of studies carried out in a 1*g* environment by Su et al. (2014).

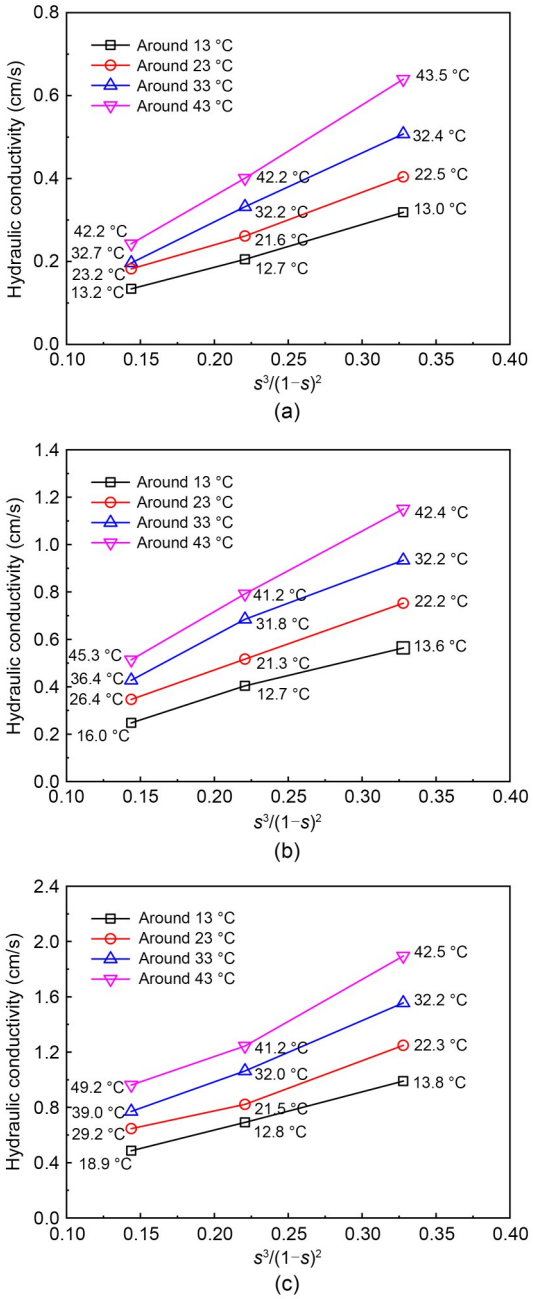

Fig. 8 Relationships between the hydraulic conductivity and the porosity function ($s^3/(1-s)^2$) of sand in similar temperature ranges under different centrifugal accelerations: (a) 15*g*; (b) 30*g*; (c) 50*g*

3.4 Quantitative analysis of the influence of multiple factors on the hydraulic conductivity of sand

Under the interaction of the centrifugal environment (*ng*), temperature (*T*), and soil porosity (*s*), the hydraulic conductivity of sand may differ from that measured in a 1*g* environment. Hydraulic conductivity has a significant impact on issues like soil consolidation and the liquefaction of sand in a centrifugal environment. Therefore, quantitative analysis of the influence of multiple factors, such as centrifugal acceleration, temperature, and porosity, on the hydraulic conductivity of sand in centrifuge modeling becomes extremely important. In this study, the hydraulic conductivity (k) was a ternary function, denoted as $k=k(n, T, s)$. Therefore, it is necessary to first establish the relationship between the hydraulic conductivity and the temperature and porosity, denoted as $k=k(T, s)$, or the relationship between the hydraulic conductivity and the centrifugal acceleration and porosity, denoted as $k=k(n, s)$. Then, the function $k=k(n, T, s)$ can be derived. In the following section, we will introduce these two methods separately.

3.4.1 Establishing $k(n, T, s)$ based on $k(T, s)$

Firstly, the hydraulic conductivities of sand samples at the real temperature in the 15*g* environment were normalized to hydraulic conductivities at 15, 25, 35, and 45 °C. The normalized process involves changing the hydraulic conductivity measured at the real temperature to the hydraulic conductivity at a particular temperature. To illustrate, the process of normalizing the hydraulic conductivity at the real temperature of 13.2 °C ($k_{13.2}$) to the hydraulic conductivity at 15 °C (k_{15}) was determined using the equation $k_{15}=k_{13.2}\times(\mu_{13.2}/\mu_{15})$, where $\mu_{13.2}$ and μ_{15} represent the dynamic viscosity coefficients of the fluid at 13.2 and 15 °C, respectively. Subsequently, the relationship between the normalized hydraulic conductivity and the porosity function $s^3/(1-s)^2$ was plotted, followed by linear regression analysis (Fig. 9). Fig. 9 shows that there was a linear positive correlation between the normalized hydraulic conductivity and the porosity function $s^3/(1-s)^2$. This means that the normalized hydraulic conductivity and the porosity function $s^3/(1-s)^2$ have the following relationship:

$$k_T=a\frac{s^3}{(1-s)^2}+b, \tag{5}$$

where parameters a and b are obtained by fitting.

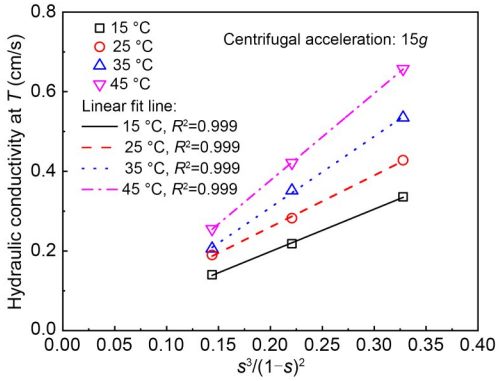

Fig. 9 Relationship between the normalized hydraulic conductivity and the porosity function $s^3/(1-s)^2$ in the 15*g* environment

The parameter a of 15*g* and temperature T have a strong linear relationship, which satisfies the following equation:

$$a=cT+d, \tag{6a}$$

where parameters c and d are obtained by linear fitting. Specifically, in this study,

$$a=0.03844T+0.4293,\ \ R^2=0.983. \tag{6b}$$

Substituting Eq. (6a) into Eq. (5), the quantitative predictive equation for the hydraulic conductivity of sand, considering the influence of multiple factors in centrifuge modeling, can be obtained:

$$k(T, s)=cT\frac{s^3}{(1-s)^2}+d\frac{s^3}{(1-s)^2}+b. \tag{7}$$

Eq. (7) is derived based on the normalized hydraulic conductivity in a 15*g* environment. To verify the applicability of Eq. (7), it was used to fit the hydraulic conductivity at actual temperatures under different centrifugal accelerations (Fig. 10). Fig. 10 shows that under various centrifugal accelerations, Eq. (7) provides good fitting results for the hydraulic conductivities at real temperatures of sand samples at different porosities.

The parameter c and the centrifugal acceleration level n satisfy

$$c=fn+j, \tag{8a}$$

where f and j are coefficients. Specifically, in this study,

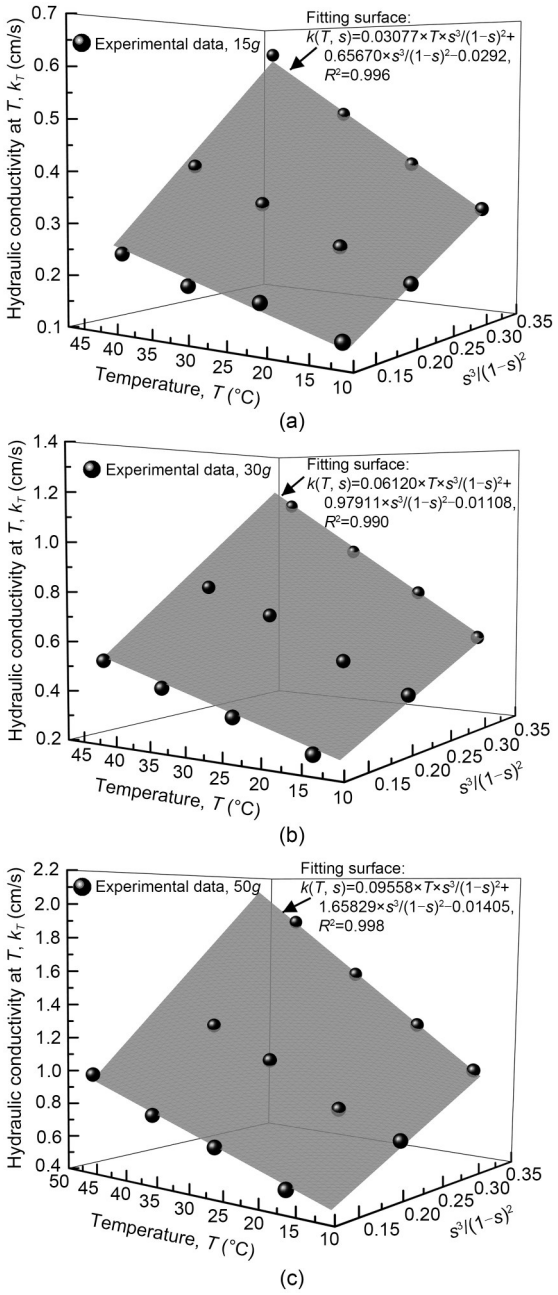

Fig. 10 Using Eq. (7) to fit the hydraulic conductivity at real temperatures under different centrifugal accelerations: (a) 15*g*; (b) 30*g*; (c) 50*g*

$$c = 0.00193n + 0.00410,\ R^2 = 0.998. \tag{8b}$$

The parameter d and the centrifugal acceleration n level satisfy

$$d = on + u, \tag{9a}$$

where o and u are coefficients. Specifically, in this study,

$$d = 0.03023n + 0.18255,\ R^2 = 0.986. \tag{9b}$$

Substituting Eqs. (8b) and (9b) into Eq. (7), we obtain

$$k(n,\ T,\ s) = 0.00193nT\frac{s^3}{(1-s)^2} + 0.00410T\frac{s^3}{(1-s)^2} + 0.03023n\frac{s^3}{(1-s)^2} + 0.18255\frac{s^3}{(1-s)^2} - 0.0292. \tag{10}$$

Hence, we have established a quantitative relationship between the hydraulic conductivity and factors such as temperature, porosity, and centrifugal acceleration level in centrifuge modeling by first establishing the relationship between the hydraulic conductivity and temperature and porosity.

3.4.2 Establishing $k(n, T, s)$ based on $k(n, s)$

Firstly, the hydraulic conductivities of sand samples around 23 °C were normalized to 25 °C. In accordance with Garnier et al. (2007), we support that there was a linear positive correlation between the normalized hydraulic conductivity and the centrifugal acceleration level:

$$k_T = a_1 n, \tag{11}$$

where a_1 is the coefficient. Subsequently, the relationship between the normalized hydraulic conductivity and centrifugal acceleration level under the same porosity was plotted, followed by linear regression analysis (Fig. 11).

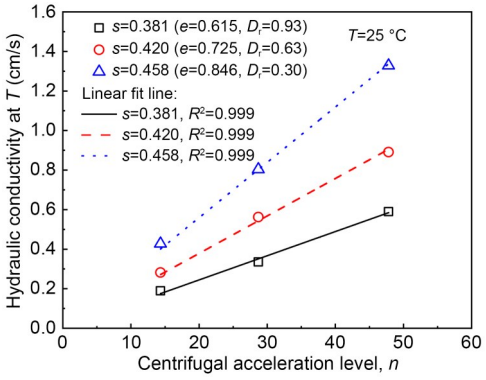

Fig. 11 Relationship between the normalized hydraulic conductivity at 25 °C and the centrifugal acceleration level

There is a linear relationship between parameter a_1 of 25 ℃ and the porosity function $s^3/(1-s)^2$, which satisfies the following equation:

$$a_1 = b_1 \frac{s^3}{(1-s)^2}, \tag{12a}$$

where parameter b_1 is obtained by linear fitting. After substituting Eq. (12a) into Eq. (11), the hydraulic conductivity and the centrifugal acceleration level still satisfy the linear positive correlation. Specifically, in this study,

$$a_1 = 0.08539 \frac{s^3}{(1-s)^2}, \ R^2 = 0.999. \tag{12b}$$

Substituting Eq. (12a) into Eq. (11), the quantitative predictive equation for the hydraulic conductivity of sand, considering the influence of multiple factors in centrifuge modeling, can be obtained:

$$k(n, s) = b_1 n \frac{s^3}{(1-s)^2}. \tag{13}$$

Eq. (13) is derived based on the normalized hydraulic conductivity. To verify the applicability of Eq. (13), it was used to fit the hydraulic conductivity at real temperatures (Fig. 12). Fig. 12 shows that Eq. (13) provides good fitting results for the hydraulic conductivities at actual temperatures of sand samples at different porosities and different centrifugal acceleration levels.

The parameter b_1 and the temperature T satisfy

$$b_1 = d_1 T + j_1, \tag{14a}$$

where d_1 and j_1 are coefficients. Specifically, in this study,

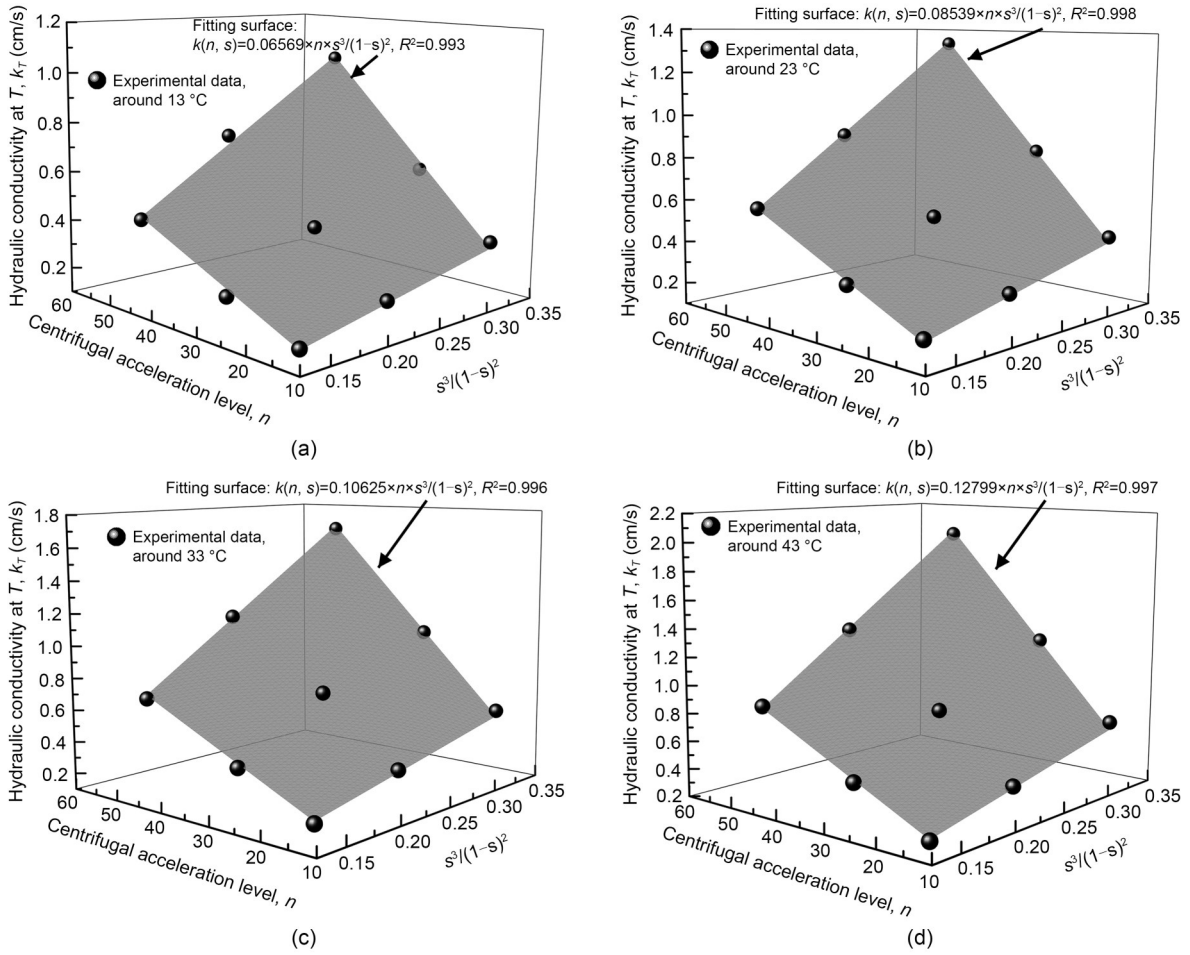

Fig. 12 Using Eq. (13) to fit the hydraulic conductivity at real temperatures: (a) around 13 ℃; (b) around 23 ℃; (c) around 33 ℃; (d) around 43 ℃

$$b_1 = 0.00208T + 0.03400,\ R^2 = 0.999. \quad (14b)$$

Substituting Eq. (14b) into Eq. (13), we obtain

$$k(n,\ T,\ s) = 0.00208nT\frac{s^3}{(1-s)^2} + 0.03400n\frac{s^3}{(1-s)^2}. \quad (15)$$

Thus, we have established a quantitative relationship between the hydraulic conductivity and factors such as temperature, porosity, and the centrifugal acceleration level, by first establishing the relationship between the hydraulic conductivity and centrifugal acceleration level and porosity.

The quantitative relationships between the hydraulic conductivity and temperature, porosity, and centrifugal acceleration level derived via the two methods, namely Eqs. (10) and (15), show some discrepancies. We will discuss these differences later.

3.5 Applicability of Kozeny-Carman equation to centrifuge modeling

In Section 3.4, based on the porosity function from the Kozeny-Carman equation, we established the relationships between the hydraulic conductivity and temperature, porosity, and centrifugal acceleration level. From this, we also inferred that the Kozeny-Carman equation may be used to predict the hydraulic conductivity of sand in a centrifugal environment. Therefore, in this section, we validate the applicability of the Kozeny-Carman equation to centrifuge modeling. The relevant parameters in the Kozeny-Carman equation (Eq. (4)) were determined as follows.

According to the particle size distribution curve of the soil samples in this study (Fig. 2), the gradation equation for the soil with diameters ranging from 0.10 to 0.25 mm is as follows:

$$y = 245.80426\lg x + 247.98890, \quad (16)$$

where y represents a percentage, and the unit of x is mm. The d_m typically uses d_{10}, d_{20}, etc. The relationship between the water's dynamic viscosity (Chen MH et al., 2019) and temperature within the range of 10 to 50 ℃ satisfies the following:

$$\mu = \frac{1}{26.42042T + 471.29372}. \quad (17)$$

In this study, we used d_{10} or d_{20}, which, according to the gradation equation (Eq. (16)), equals 0.108 mm or 0.118 mm, respectively. Substituting d_m and Eq. (17) into Eq. (4) and considering the influence of the centrifugal environment (that is, multiplied by n), the Kozeny-Carman equation is obtained as follows:

When d_m is d_{10},

$$k(n,\ T,\ s) = 0.00168nT\frac{s^3}{(1-s)^2} + 0.02993n\frac{s^3}{(1-s)^2}. \quad (18a)$$

When d_m is d_{20},

$$k(n,\ T,\ s) = 0.00200nT\frac{s^3}{(1-s)^2} + 0.03573n\frac{s^3}{(1-s)^2}. \quad (18b)$$

Eq. (18b) is essentially similar in form to Eq. (15). Thus, we believe that the Kozeny-Carman equation can accurately estimate the hydraulic conductivity of sand in centrifuge modeling under the various experimental conditions of this study. However, its applicability to a wider range of test conditions requires further study, as discussed in Section 3.6.

3.6 Discussion

Table 2 presents the hydraulic conductivity prediction equation of sand in centrifuge modeling that was obtained in this study. First, we discuss the reasons

Table 2 Summary of prediction equations

Equation	Specific expression
Eq. (10)	$k(n,\ T,\ s) = 0.00193nT\frac{s^3}{(1-s)^2} + 0.00410T\frac{s^3}{(1-s)^2} + 0.03023n\frac{s^3}{(1-s)^2} + 0.18255\frac{s^3}{(1-s)^2} - 0.0292$
Eq. (15)	$k(n,\ T,\ s) = 0.00208nT\frac{s^3}{(1-s)^2} + 0.03400n\frac{s^3}{(1-s)^2}$
Eq. (18b)	$k(n,\ T,\ s) = 0.00200nT\frac{s^3}{(1-s)^2} + 0.03573n\frac{s^3}{(1-s)^2}$

for the differences between Eqs. (10) and (15) as well as Eq. (18b). Comparing Eq. (10) with Eq. (15), it is evident that Eq. (15) is missing three terms, specifically $0.00410Ts^3/(1-s)^2$, $0.18255s^3/(1-s)^2$, and -0.0292. The occurrence of -0.0292 is due to the parameter b in Eq. (5), and when porosity s tends to 0, b tends to 0. Fig. 10 shows also that the corresponding values of b for 15g, 30g, and 50g are -0.0292, 0.01108, and 0.01405, respectively. When compared with the actual hydraulic conductivity, this term can be considered negligible. There are still two missing terms, specifically $0.00410Ts^3/(1-s)^2$ and $0.18255s^3/(1-s)^2$. The discrepancy may be attributed to our assumption in obtaining Eq. (15) that the hydraulic conductivity of soil is directly proportional to the centrifugal acceleration level, as stated in Eq. (11). Some studies (Singh and Gupta, 2000; Wang et al., 2011) have shown that the hydraulic conductivity of soil in centrifuge modeling exhibits a direct correlation with n^{χ}, where χ is close to 1, which may be due to the soil's re-compression in a centrifugal environment. Hence, while applying Eq. (11) for fitting, there may be a certain degree of error. Meanwhile, considering that the coefficients in Eq. (18b) were obtained from parameters under a 1g scaling without considering the influence of the centrifugal environment, overall, Eq. (10) is closer to the actual situation in centrifuge modeling than Eqs. (15) and (18b). Eq. (10) more comprehensively considers the influence of factors such as the centrifugal environment, and thus is more suitable for predicting the hydraulic conductivity of sand in centrifugal tests.

As previously stated, in the specific experimental settings of this study (with a temperature range of 12 to 49 °C and a maximum centrifugal acceleration of 50g), Eqs. (15) and (18b), similar to Eq. (10), would exhibit accurate prediction capabilities. However, for larger centrifugal accelerations and higher temperatures, the predictive performance of Eqs. (15) and (18b) is unclear. Therefore, we compared the hydraulic conductivities calculated by Eqs. (10), (15), and (18b) under higher temperatures (up to 60 °C) (Ko et al., 2013) and greater centrifugal accelerations (up to 350g) (Hou and Wang, 2023). Fig. 13 shows the hydraulic conductivities calculated by Eqs. (10), (15), and (18b) at different temperatures plotted against the centrifugal acceleration level. Since the phenomena under the two other porosities are consistent with those at a porosity of 0.420, only the figure for a porosity of 0.420 is provided.

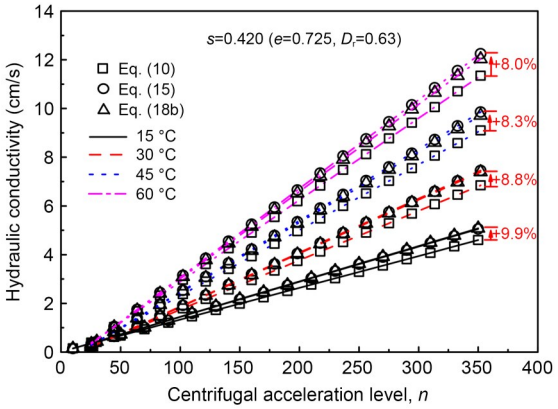

Fig. 13 Variation of hydraulic conductivities calculated by Eqs. (10), (15), and (18b) with centrifugal acceleration level

Fig. 13 shows that at the same temperature, when the centrifugal acceleration is less than 50g, the hydraulic conductivities calculated by the above three equations are relatively close. This is because when the centrifugal acceleration is less than 50g, the soil compression caused by the centrifugal environment is minimal. Even though Eqs. (15) and (18b) do not fully consider the influence of the centrifugal environment on the hydraulic conductivity of sand, the results obtained from them are very close to those obtained from Eq. (10), which is consistent with the conclusions of this study. Therefore, when the centrifugal acceleration is less than 50g, all three equations above can be used. When the centrifugal acceleration exceeds 50g, the hydraulic conductivities calculated by Eqs. (15) and (18b) start to significantly exceed those calculated by Eq. (10), and as the centrifugal acceleration increases, this phenomenon becomes more pronounced. For example, at 15, 30, 45, and 60 °C, the hydraulic conductivities at 350g calculated by Eq. (15) are respectively 9.9%, 8.8%, 8.3%, and 8.0% higher than those calculated by Eq. (10). This is because when the centrifugal acceleration exceeds 50g, the soil compression caused by the centrifugal environment becomes increasingly significant. As Eqs. (15) and (18b) do not fully consider the influence of the centrifugal environment on hydraulic conductivity, significant discrepancies start to appear compared to the results obtained by Eq. (10). Therefore, when the centrifugal acceleration exceeds 50g, it is recommended to prioritize the use of Eq. (10). Of course, Eqs. (15) and (18b) can still be used, but the associated errors must be considered.

4 Conclusions

In this study, we used a temperature-controlled falling-head permeameter apparatus to conduct centrifuge modeling. A series of falling-head seepage tests were performed on sand samples with various porosities at different temperatures and centrifugal accelerations. Based on the results, the following conclusions were made:

(1) The centrifuge test results show that in a similar temperature range, no matter how dense the sand, the hydraulic conductivity of the sand is linearly correlated with centrifugal acceleration; when subjected to the same centrifugal acceleration and in a similar temperature range, the hydraulic conductivity of the sand exhibits an almost linear increase in relation to its porosity function ($s^3/(1-s)^2$).

(2) Two pathways were used to obtain functional equations for the hydraulic conductivity of the sand in centrifuge modeling, considering the influencing factors of temperature (T), centrifugal acceleration level (n), and porosity (s). The functional equation obtained by the first pathway is Eq. (10), and the functional equation obtained by the second pathway is Eq. (15).

(3) We assessed the applicability of the specific expression of the Kozeny-Carman equation in this study (Eq. (18b)), as well as Eqs. (15) and (10). When the centrifugal acceleration is less than 50g, the three equations are highly reliable for forecasting the hydraulic conductivity of sand. When the centrifugal acceleration exceeds 50g, it is advisable to give priority to the use of Eq. (10). Eqs. (15) and (18b) can still be used, but their associated errors must be considered.

Acknowledgments

This work is supported by the Basic Science Center Program for Multiphase Media Evolution in Hypergravity of the National Natural Science Foundation of China (No. 51988101).

Author contributions

Conceptualization contributed by Jianjian HE and Yubing WANG; methodology by Jianjian HE and Xihao JIANG; data collection by Jianjian HE and Xihao JIANG; formal analysis and investigation by Jianjian HE and Yubing WANG; funding acquisition by Yubing WANG; supervision by Yubing WANG. The first draft of the manuscript was written by Jianjian HE, and all authors read and approved the final version.

Data availability

The datasets generated and/or analyzed during the current study are available from the corresponding author on reasonable request.

Conflict of interest

Jianjian HE, Xihao JIANG, and Yubing WANG declare that they have no conflict of interest.

References

Aubertin M, Bussiere B, Chapuis RP, 1996. Hydraulic conductivity of homogenized tailings from hard rock mines. *Canadian Geotechnical Journal*, 33(3):470-482. https://doi.org/10.1139/t96-068

Butterfield R, 2000. Scale-modelling of fluid flow in geotechnical centrifuges. *Soils and Foundations*, 40(6):39-45. https://doi.org/10.3208/sandf.40.6_39

Carman PC, 1939. Permeability of saturated sands, soils and clays. *The Journal of Agricultural Science*, 29(2):262-273. https://doi.org/10.1017/S0021859600051789

Chapuis RP, 2004. Predicting the saturated hydraulic conductivity of sand and gravel using effective diameter and void ratio. *Canadian Geotechnical Journal*, 41(5):787-795. https://doi.org/10.1139/t04-022

Chen MH, Pan HL, Qi MZ, 2019. Principles of Chemical Engineering, 3rd Edition. East China University of Science and Technology Press, Shanghai, China, p.278-279 (in Chinese).

Chen YL, Irfan M, Uchimura T, et al., 2019. Development of elastic wave velocity threshold for rainfall-induced landslide prediction and early warning. *Landslides*, 16(5):955-968. https://doi.org/10.1007/s10346-019-01138-2

Chen YM, Han C, Ling DS, et al., 2011. Development of geotechnical centrifuge ZJU400 and performance assessment of its shaking table system. *Chinese Journal of Geotechnical Engineering*, 33(12):1887-1894 (in Chinese).

Cheng C, Jia PJ, Ni PP, et al., 2023. Upper bound analysis of longitudinally inclined EPB shield tunnel face stability in dense sand strata. *Transportation Geotechnics*, 41:101031. https://doi.org/10.1016/j.trgeo.2023.101031

Cho WJ, Lee JO, Chun KS, 1999. The temperature effects on hydraulic conductivity of compacted bentonite. *Applied Clay Science*, 14(1-3):47-58. https://doi.org/10.1016/S0169-1317(98)00047-7

Eisma JA, Merwade VM, 2020. Investigating the environmental response to water harvesting structures: a field study in Tanzania. *Hydrology and Earth System Sciences*, 24(4): 1891-1906. https://doi.org/10.5194/hess-24-1891-2020

Fan JY, Rowe RK, 2024. An empirical equation predicting the saturated hydraulic conductivity of tailings. *Canadian Geotechnical Journal*, 61(9):2042-2047. https://doi.org/10.1139/cgj-2023-0339

Flint LE, Selker JS, 2003. Use of porosity to estimate hydraulic properties of volcanic tuffs. *Advances in Water Resources*, 26(5):561-571. https://doi.org/10.1016/S0309-1708(02)00182-3

Gao XH, Tian WP, Li JC, et al., 2023. Research on the stress and deformation characteristics of circular foundation pit during excavation in sand soil. *Advances in Materials Science and Engineering*, 2023:3008695. https://doi.org/10.1155/2023/3008695

Garnier J, Gaudin C, Springman SM, et al., 2007. Catalogue of scaling laws and similitude questions in geotechnical centrifuge modelling. *International Journal of Physical Modelling in Geotechnics*, 7(3):1-23. https://doi.org/10.1680/ijpmg.2007.070301

Hou YJ, Wang X, 2023. Construction and operation of geotechnical centrifuge laboratories. *Chinese Journal of Geotechnical Engineering*, 45(11):2396-2402 (in Chinese). https://doi.org/10.11779/CJGE20210909

Ikbarieh A, Izadifar M, Abu-Farsakh MY, et al., 2023. A parametric study of embankment supported by geosynthetic reinforced load transfer platform and timber piles tip on sand. *Transportation Geotechnics*, 38:100901. https://doi.org/10.1016/j.trgeo.2022.100901

Joshaghani M, Ghasemi-Fare O, 2021. Exploring the effects of temperature on intrinsic permeability and void ratio alteration through temperature-controlled experiments. *Engineering Geology*, 293:106299. https://doi.org/10.1016/j.enggeo.2021.106299

Khalajzadeh AK, Choobbasti AJ, Kutenaei SS, 2023. Dynamic behaviour of a circular tunnel in the sand: a numerical verification of a centrifuge program. *Tunnelling and Underground Space Technology*, 138:105152. https://doi.org/10.1016/j.tust.2023.105152

Ko JH, Powell J, Jain P, et al., 2013. Case study of controlled air addition into landfilled municipal solid waste: design, operation, and control. *Journal of Hazardous, Toxic, and Radioactive Waste*, 17(4):351-359. https://doi.org/10.1061/(ASCE)HZ.2153-5515.0000183

Li LX, Fu QH, Huang JJ, 2018. Centrifuge model tests on cantilever foundation pit engineering in sand ground and silty clay ground. *Rock and Soil Mechanics*, 39(2):529-536 (in Chinese). https://doi.org/10.16285/j.rsm.2016.0333

Li PN, Xu YS, Wang XW, 2023. Estimation of hydraulic conductivity by the modified Kozeny-Carman equation considering the derivation principle of the original equation. *Journal of Hydrology*, 621:129658. https://doi.org/10.1016/j.jhydrol.2023.129658

Li XD, Qiu YY, Li HJ, et al., 2024. Influence of impact load on permeability of saturated calcareous sand. *Marine Georesources & Geotechnology*, 42(3):223-232. https://doi.org/10.1080/1064119X.2023.2168577

Li YL, Tian C, Wen LF, et al., 2021. A study of the overtopping breach of a sand-gravel embankment dam using experimental models. *Engineering Failure Analysis*, 124:105360. https://doi.org/10.1016/j.engfailanal.2021.105360

Ling H, Ling I, 2012. Centrifuge model simulations of rainfall-induced slope instability. *Journal of Geotechnical and Geoenvironmental Engineering*, 138(9):1151-1157. https://doi.org/10.1061/(ASCE)GT.1943-5606.0000679

Mei SY, Zhong QM, Chen SS, et al., 2022. Investigation of the overtopping-induced breach of tailings dams. *Computers and Geotechnics*, 149:104864. https://doi.org/10.1016/j.compgeo.2022.104864

Ng CWW, 2014. The state-of-the-art centrifuge modelling of geotechnical problems at HKUST. *Journal of Zhejiang University-SCIENCE A (Applied Physics & Engineering)*, 15(1):1-21. https://doi.org/10.1631/jzus.A1300217

Ng CWW, Coo JL, 2015. Hydraulic conductivity of clay mixed with nanomaterials. *Canadian Geotechnical Journal*, 52(6):808-811. https://doi.org/10.1139/cgj-2014-0313

Ng CWW, Farivar A, Gomaa SMMH, et al., 2021. Centrifuge modeling of cyclic nonsymmetrical thermally loaded energy pile groups in clay. *Journal of Geotechnical and Geoenvironmental Engineering*, 147(12):04021146. https://doi.org/10.1061/(ASCE)GT.1943-5606.0002689

Nomura S, Yamamoto Y, Sakaguchi H, 2018. Modified expression of Kozeny-Carman equation based on semilog-sigmoid function. *Soils and Foundations*, 58(6):1350-1357. https://doi.org/10.1016/j.sandf.2018.07.011

Qin CJ, Hazarika H, Liu GJ, et al., 2024. Seismic behavior of highway embankment reinforced with remedial countermeasures on saturated loose sandy layer. *Transportation Geotechnics*, 45:101183. https://doi.org/10.1016/j.trgeo.2024.101183

Sailer E, Taborda DMG, Zdravković L, et al., 2021. Thermo-hydro-mechanical interactions in porous media: implications on thermo-active retaining walls. *Computers and Geotechnics*, 135:104121. https://doi.org/10.1016/j.compgeo.2021.104121

Schofield AN, 1980. Cambridge geotechnical centrifuge operations. *Géotechnique*, 30(3):227-268. https://doi.org/10.1680/geot.1980.30.3.227

Sharma JS, Samarasekera L, 2007. Effect of centrifuge radius on hydraulic conductivity measured in a falling-head test. *Canadian Geotechnical Journal*, 44(1):96-102. https://doi.org/10.1139/t06-092

Singh DN, Gupta AK, 2000. Modelling hydraulic conductivity in a small centrifuge. *Canadian Geotechnical Journal*, 37(5):1150-1155. https://doi.org/10.1139/t00-027

Su LJ, Zhang YJ, Wang TX, 2014. Investigation on permeability of sands with different particle sizes. *Rock and Soil Mechanics*, 35(5):1289-1294 (in Chinese). https://doi.org/10.16285/j.rsm.2014.05.034

Sun Y, Zhao Y, Zhang DL, 2019. Surface subsidence of pit-in-pit foundation in sand-cobble stratum in Beijing area. *Proceedings of the Institution of Civil Engineers-Ground Improvement*, 172(2):96-107. https://doi.org/10.1680/jgrim.17.00037

Tan TS, Scott RF, 1985. Centrifuge scaling considerations for fluid-particle systems. *Géotechnique*, 35(4):461-470. https://doi.org/10.1680/geot.1985.35.4.461

Tan TS, Scott RF, 1987. Discussion: centrifuge scaling considerations for fluid-particle systems. *Géotechnique*, 37(1):131-133. https://doi.org/10.1680/geot.1987.37.1.131

Thusyanthan NI, Madabhushi SPG, 2003. Scaling of seepage

flow velocity in centrifuge models. *Acta Gastroenterologica Latinoamericana*, 38(2):105-115.

van Tonder WD, Jacobsz SW, 2017. Seepage column hydraulic conductivity tests in the geotechnical centrifuge. *Journal of the South African Institution of Civil Engineering*, 59(3):16-24. https://doi.org/10.17159/2309-8775/2017/v59n3a3

Wang LJ, Zhu B, Chen YM, et al., 2022. Centrifuge modelling on behaviour of hydrate bearing sediments during gas production by depressurization. Proceedings of the 10th International Conference on Physical Modelling in Geotechnics, p.495-499.

Wang NX, Zhang WM, Gu XW, et al., 2013. Centrifugal model test on seepage characteristics of high core rockfill dam. *Rock and Soil Mechanics*, 34(10):2769-2773 (in Chinese).

Wang QS, Chen ZY, Sui HB, et al., 2011. Modelling seepage flow velocity in centrifuge models. *Chinese Journal of Geotechnical Engineering*, 33(8):1235-1239 (in Chinese).

Wang Y, Shi B, Gao L, et al., 2010. Laboratory tests for temperature effects of clayey soil permeability. *Journal of Engineering Geology*, 18(3):351-356 (in Chinese). https://doi.org/10.3969/j.issn.1004-9665.2010.03.010

Wang Y, Ren YB, Yang Q, 2017. Experimental study on the hydraulic conductivity of calcareous sand in South China Sea. *Marine Georesources & Geotechnology*, 35(7):1037-1047. https://doi.org/10.1080/1064119X.2017.1279245

Wen LF, Chai JR, Wang X, et al., 2015. Behaviour of concrete-face rockfill dam on sand and gravel foundation. *Proceedings of the Institution of Civil Engineers-Geotechnical Engineering*, 168(5):439-456. https://doi.org/10.1680/jgeen.14.00103

Xiong ZC, 2018. Analysis for Heat Transfer and Multi-Field Coupling of Energy Geostructures. MS Thesis, Tsinghua University, Beijing, China (in Chinese).

Yang YS, Yu HT, Yuan Y, et al., 2021. 1*g* shaking table test of segmental tunnel in sand under near-fault motions. *Tunnelling and Underground Space Technology*, 115:104080. https://doi.org/10.1016/j.tust.2021.104080

Ye W, Hu J, Ma FH, 2021. Centrifuge model study on the influence of desiccation cracks on the seepage behavior of upstream clay anti-seepage system subjected to abrupt flood. *Bulletin of Engineering Geology and the Environment*, 80(6):5075-5090. https://doi.org/10.1007/s10064-021-02207-4

Ye WM, Wan M, Chen B, et al., 2013. Temperature effects on the swelling pressure and saturated hydraulic conductivity of the compacted GMZ01 bentonite. *Environmental Earth Sciences*, 68(1):281-288. https://doi.org/10.1007/s12665-012-1738-4

Ye ZG, Wang LJ, Zhu B, et al., 2022. A thermo-hydro-chemo-mechanical coupled model for natural gas hydrate-bearing sediments considering gravity effect. *Journal of Natural Gas Science and Engineering*, 108:104823. https://doi.org/10.1016/j.jngse.2022.104823

Zeng X, Su J, Wang HY, et al., 2022. Centrifuge modeling of chloride ions completely breakthrough kaolin clay liner. *Sustainability*, 14(12):6976. https://doi.org/10.3390/su14126976

Zhang LC, Zhong QM, Yang M, et al., 2023. Centrifugal model tests on overtopping-induced breaching of landslide dams. *Chinese Journal of Geotechnical Engineering*, 45(S1): 197-200 (in Chinese). https://doi.org/10.11779/CJGE2023S10029

Zhao JB, Chen L, Collin F, et al., 2016. Numerical modeling of coupled thermal-hydro-mechanical behavior of GMZ bentonite in the China-mock-up test. *Engineering Geology*, 214:116-126. https://doi.org/10.1016/j.enggeo.2016.09.015

Zhao YY, Yang Y, Ling XZ, et al., 2021. Dynamic behavior of natural sand soils and fiber reinforced soils in heavy-haul railway embankment under multistage cyclic loading. *Transportation Geotechnics*, 28:100507. https://doi.org/10.1016/j.trgeo.2020.100507

Zheng J, Li YC, Ke H, et al., 2022. Centrifuge and numerical modeling of the impact of sediment consolidation induced by capping on contaminant transportation. *Bulletin of Engineering Geology and the Environment*, 81(11):487. https://doi.org/10.1007/s10064-022-02986-4

Zhong Y, Zhou AN, Du JP, et al., 2023. Modified Kozeny-Carman equation for estimating hydraulic conductivity in nanoscale pores of clayey soils with active surfaces. *Journal of Hydrology*, 626:130209. https://doi.org/10.1016/j.jhydrol.2023.130209

Zhu ZH, Zhang F, Dupla JC, et al., 2021. Assessment of tamping-based specimen preparation methods on static liquefaction of loose silty sand. *Soil Dynamics and Earthquake Engineering*, 143:106592. https://doi.org/10.1016/j.soildyn.2021.106592